This is a non-peer reviewed preprint submitted to EarthArXiv.

This is a non-peer reviewed preprint submitted to EarthArXiv. This manuscript has been submitted to *Earth, Planets and Space*.

# Title: Co- and postseismic slip behaviors extracted from decadal seafloor geodesy after the 2011 Tohoku-oki earthquake

Author #1: Shun-ichi Watanabe, Hydrographic and Oceanographic Department, Japan Coast Guard, 3-1-1, Kasumigaseki, Chiyoda-ku, Tokyo, 100-8932, Japan, s-watanabe@jodc.go.jp

Author #2: Tadashi Ishikawa, Hydrographic and Oceanographic Department, Japan Coast Guard, 3-1-1, Kasumigaseki, Chiyoda-ku, Tokyo, 100-8932, Japan, ishikawa@jodc.go.jp

Author #3: Yuto Nakamura, Hydrographic and Oceanographic Department, Japan Coast Guard, 3-1-1, Kasumigaseki, Chiyoda-ku, Tokyo, 100-8932, Japan, ynakamura@jodc.go.jp

Author #4: Yusuke Yokota, Institute of Industrial Science, University of Tokyo; 4-6-1, Komaba, Meguro-ku, Tokyo, 153-8505, Japan, yyokota@iis.u-tokyo.ac.jp

**Corresponding author #1**

This is a non-peer reviewed preprint submitted to EarthArXiv.


## Abstract

Investigations of the co- and postseismic processes of the 2011 Tohoku-oki earthquake provide essential information on the seismic cycle in the Japan Trench. Although various postseismic models have been proposed, no consensus has been reached, especially on the along-strike extensions of the main rupture due to the lack of conclusive evidence, even in the coseismic process. To decompose the postseismic transient processes in and around the source region, i.e., viscoelastic relaxation and afterslip, long-term postseismic geodetic observation on the seafloor plays an essential role. Here, from decadal seafloor geodetic data, we provide empirical evidence for offshore aseismic afterslip on the rupture edges that had almost decayed within 2–3 year. The afterslip regions are considered to have stopped the north-south rupture propagation. In the southern source region (~37 °N), despite not resolved by coseismic geodetic data, shallow tsunamigenic slip near the trench is captured by postseismic seafloor geodesy as a subsequent viscoelastic deformation causing persistent seafloor subsidence at a geodetic site off-Fukushima. After a decade from the earthquake, the

long-term viscoelastic relaxation process is currently in progress and is still dominant in the rupture area.

## Keywords

2011 Tohoku-oki earthquake; GNSS-A; seafloor geodesy; Postseismic crustal deformation; Shallow tsunamigenic slip; Afterslip; Viscoelastic relaxation

# Main Text

### 1 Introduction

In general, a large fault rupture is followed by postseismic relaxation processes such as viscoelastic relaxation in the asthenosphere and aseismic slip on the fault plane, which lead to transient crustal deformation on the solid Earth's surface (e.g., Wang et al., 2012). Postseismic geodetic data following a megathrust earthquake show the sum of these relaxation processes and interplate backslip due to the secular plate subduction. Along the Japan Trench, postseismic processes were triggered by the 2011 Tohoku-oki earthquake ($M_w$ 9.0) and continue in this decade. Clarifying the interplate slip behaviors for the co- and postseisimic phase will contribute to the understanding of the frictional state of faults, slow earthquake activities, and seismic cycles in this region.

The Tohoku-oki earthquake caused trench-ward seafloor displacements of several tens of meters (Sato et al., 2011; Kido et al., 2011), reaching about 50 m at the trench (Fujiwara et al., 2011). Using seafloor geodetic data (Sato et al., 2011; Kido et al., 2011), which provided definitive evidence for a coseismic slip, an extremely large slip was estimated at the plate interface shallower than the hypocenter (Figure 1) (Ozawa et al., 2012; Iinuma et al., 2012; Sun et al., 2017; Wang et al., 2018). Except for the north-south spread of shallow rupture, where the geodetic data at that time could not resolve the slips, a consensus has been reached on the north-south rupture propagation at depths near the hypocenter; almost all fault models produce similar results as summarized by Sun et al. (2017) and Wang et al. (2018). This implies that the rupture in 2011 did not progress to the northern region (> 39 °N), even though $M_w$ 8 earthquakes have historically occurred in this region (Figure 1) (Nagai et al., 2001; Yamanaka and Kikuchi, 2004). Investigations of the postseismic behaviors, including the occurrence of afterslip, in the northern and southern regions outside the main rupture area provide

This is a non-peer reviewed preprint submitted to EarthArXiv.

essential information on how rupture propagation was restrained in a compact region in the depths near the hypocenter.

For the detection of transient postseismic crustal deformation to decompose the elementary processes, sufficiently long-term, high-frequency, and well-distributed geodetic data are required because these sources have different decay times and deformation patterns (e.g., Wang et al., 2012). Although the terrestrial Global Navigation Satellite System (GNSS) observation network has extremely high spatiotemporal resolution, it cannot easily decompose the transient processes because the two processes of interest cause similar trench-ward movements in the onshore regions and thus cannot be distinguished from one another. In contrast, the viscoelastic and afterslip effects cause displacements in opposite directions on the seafloor above the main rupture, i.e., the landward and trench-ward directions, respectively. Therefore, seafloor geodetic observations can be used to decompose transient deformation sources despite their lower temporal resolution compared to that of terrestrial observations. Actually, seafloor geodetic technique detected postseismic landward movements larger than the subduction rate (~ 9 cm/year) (Argus et al., 2011) above the main rupture area,

This is a non-peer reviewed preprint submitted to EarthArXiv.

whereas terrestrial geodetic sites showed trench-ward movements. This is a conclusive evidence for the dominance of viscoelastic relaxation in the main rupture area (Watanabe et al., 2014; Sun et al. 2014; Tomita et al., 2017; Honsho et al., 2019).

The seafloor observation results stimulated researchers to develop postseismic deformation models incorporating the viscoelastic effects. Table 1 summarizes the postseismic models with (1) referencing the seafloor geodetic data, (2) incorporating the afterslip dislocation models, (3) modeling the subducting cold slab, and (4) calculating the viscoelastic deformation in wider area than a latitude range of 37–39 °N. Every model indicated that the deformation patterns in the main rupture area can be roughly explained as the viscoelastic response, but that the observed deformation in the outside of main rupture cannot be reproduced only by viscoelastic relaxation. Some models put additional afterslip patches in the offshore region to reproduce the geodetic data (e.g., Sun and Wang., 2015; Freed et al., 2017), even though these were only the tentative models because of the insufficient spatiotemporal resolution and observation period (at most 5 years) of available seafloor data.

On the other hand, there remains an uncertainty in coseismic dislocation input for the postseismic deformation modeling. Many researchers had adopted coseismic slip distribution model inverted from seafloor and terrestrial geodetic data with roughness dumping (e.g., Iinuma et al., 2012; Freed et al., 2017), though the geodetic network in 2011 did not cover the whole source region, for which there is thus no information especially on coseismic rupture in the shallower portion. Tsunami data, which are sensitive to topographical changes of the seafloor, indicate that the tsunamigenic area was extended, especially in the northern (> 39 °N) and southern (~37 °N) areas along the trench (Figure 1) (Satake et al., 2013). This feature did not appear in the geodetic inversion due to the absence of data. Nonetheless, the difference in coseismic input would affect the postseismic relaxation processes. For instance, a viscoelastic model proposed by Agata et al. (2019), where an output of seismic cycle simulation (Nakata et al., 2016) that included an additional shallow slip near the trench eastern off-Fukushima (~37 °N) is applied to the coseismic input, suggested that viscoelastic relaxation can cause significant seafloor deformation in the off-Fukushima region, whereas other models based on the geodetic coseismic input could not induce enough stress to cause significant viscoelastic deformation there (e.g., Sun et al., 2014; Freed et al., 2017). The difference between models suggests that we will be able to estimate shallow coseismic slip behavior and following postseismic models by decomposing and discussing the postseismic deformation sources with longer-term seafloor geodetic data.

In this study, decadal seafloor geodetic data that contain the temporal evolutions of surface velocity are used to decompose the deformation sources. Based on the results, we clarify the co- and postseismic slip behaviors in the northern and southern parts of the source region.

## 2 Data and Methods

To investigate the temporal evolution of seafloor crustal deformation, the Japan Coast Guard (JCG) regularly performs seafloor geodetic observations using GNSS – acoustic ranging combined seafloor positioning system (GNSS-A) (Additional file 1: Figure S1), in the Japan Trench region (e.g., Watanabe et al., 2020). GNSS-A data were obtained at six JCG sites (KAMN, KAMS, MYGI, MYGW, FUKU, and CHOS; Table S1) from March 2011 to June 2020 using survey vessels, and were processed with GARPOS v1.0.0 (Watanabe et al., 2021d). Note that the newer analysis method, which incorporated the estimation process for spatially gradient sound speed structure, has been applied to the previously published data (Watanabe et al., 2014). The JCG also performed GNSS-A observations at five sites (G08, G10, G12, G14, and G17; Table S1) installed by Tohoku University (TU) (Kido et al., 2015) since 2013, independently of TU. We additionally reprocessed the GNSS-A data before the Tohoku-oki earthquake at five JCG sites (Sato et al., 2013a) using the present analysis method to determine the preseismic seafloor velocities.

All GNSS-A data used in this study are available at Zenodo (Watanabe et al., 2021a;b). Note that the GNSS-A data before 2009 were obtained by drifting observations (Additional file 1: Figure S1a), which are less precise than the recent results obtained by sailing observations (Sato et al., 2013b; Ishikawa et al., 2020).

To extract the annual-scale velocity changes, we took the following steps: We first subtract the effects of aftershocks that can cause coseismic displacement of more than 1 cm at seafloor sites (sources are shown in Figure 1), applying the method of Okada (1992). We used the Centroid Moment Tensor (CMT) solution catalogue provided by the Japan Meteorological Agency, which are available online (https://www.data.jma.go.jp/svd/eqev/data/bulletin/index_e.html). We then smoothen the time series of postseismic displacements, $x(t)$, where $t$ denotes the time after the event, by fitting with a function which are modified from the fitting curve of Tobita et al. (2017), i.e.,

$$x(t) = x_0 + vt + \alpha_1 \log\left(1 + \frac{t}{\tau_1}\right) + \alpha_2 \log\left(1 + \frac{t}{\tau_2}\right),$$

where $x_0$, $v$, $\alpha_1$ and $\alpha_2$ are estimation parameters. For the time constants $\tau_1$ and $\tau_2$, we applied the values of Fujiwara et al. (2021), i.e., $\tau_1 = 2.1176$ day and $\tau_2 = 287.45$ day, because the GNSS-A observation frequency is as low as several times per year per site which is insufficient to determine these parameters. Additionally, we approximated the exponential term in their formulation to a linear component, $vt$, because of extremely large time constant found by Fujiwara et al. (2021). It should also be noted that we put $\alpha_1 = 0$ for the TU sites where the observation started in 2013.

## 3 Results

Time series of post- and preseismic seafloor displacements with respect to the Okhotsk plate of NNR-MORVEL56 model (Argus et al., 2011) within a framework of the International Terrestrial Reference Frame 2014 (Altamimi et al., 2016; 2017) are shown in Figures 2 and S2 (Additional file 1), respectively. The values of the displacement, without corrections for aftershocks, are available at Zenodo (Watanabe et al., 2021c). To discuss the motion changes over several years, we extracted 3-year cumulative movements from the fitted curves for the periods of Apr. 2011 – Apr. 2014, Apr. 2014 – Apr. 2017, and Apr. 2017 – Apr. 2020 (Table 2, Figure 1). For the preseismic period, we only consider the average velocity (Table 2, Figure 1a).

The GNSS-A results at the TU sites independently operated by the TU research group (Kido et al., 2015; Honsho et al., 2019) are simultaneously plotted in Figures 2g–2k for comparison. The offsets in the results between two observation systems, i.e., JCG and TU, were estimated and corrected as follows: We first estimated the linear trend of JCG's results in the period of 2013–2017, and detrended both series. Offsets were calculated from the average of differences in the detrended results for 2013–2017. Text S1 (Additional file 1) describes the validations for data at G17, which has lower positioning precision that the other sites.

## 4 Discussions

Based on the temporal changes of seafloor movement (Figure 1), we discuss the expressions of viscoelastic relaxation and afterslip in the northern (off-Kamaishi), central (off-Miyagi/main rupture), and southern (off-Fukushima and off-Choshi) parts of the source region, which are conceptually illustrated in Figure 3.

In previous studies that analyzed the data until 2014 (Watanabe et al., 2014; Sun et al. 2014), landward movements at rates larger than the Pacific plate subduction were detected at the sites located above the main rupture, i.e., KAMS and MYGI (Figure 1b). This was interpreted as the superposition of the effects of viscoelastic relaxation in the asthenosphere beneath the Pacific plate, and the interplate backslip if the interplate coupling was restored (Figure 3b). Crustal deformation in this area was consistent with the quantitative models incorporating the viscoelastic response to the geodetically constrained coseismic input (Sun et al. 2014; Sun and Wang, 2015; Freed et al., 2017; Wang et al., 2018). The large landward movements at these sites continued with a slight decay over the whole period, as well as at G08, G10, G12, and G14 (Figure 1c). The

This is a non-peer reviewed preprint submitted to EarthArXiv.

decay of landward motion can be explained as the time-dependent viscoelastic deformation (Figure 3b).

Little temporal change in the present decade was found in the horizontal movement at MYGW on the downdip edge of the main rupture (Figures 1b–1d). If the interplate coupling in the main rupture had been restored, its landward motion should be canceled by a trench-ward motion driven by viscoelastic relaxation or afterslip to maintain balance for almost 10 years. Although the landward motion cannot be clearly detected, it seems to have been slightly restored after 2017. This might indicate a decrease in the dominance of relaxation processes similar to those in the main rupture area (Figure 3b).

At the northern edge of the main rupture, little horizontal displacement was observed until 2014 at KAMN (Figure 1b). Because viscoelastic relaxation is mainly driven by the stress induced in the low-viscosity layer beneath the lithosphere, it tends to cause almost the same movements at KAMN and KAMS which are only 30 km apart. To explain the velocity contrast at KAMN and KAMS, some postseismic models require afterslip to reach the trench on the northern side of the main rupture to cause a relative trench-ward motion at KAMN with respect to KAMS (Sun and Wang, 2015; Freed et al., 2017).

After 2014, landward motion significantly accelerated at KAMN and had almost the same velocity at KAMS and MYGI (Figure 1c). With the preseismic velocities (Figure 1a) taken into account, the consistency in the movements at KAMN and KAMS after 2014 indicates that the two sites have been similarly influenced by long-term viscoelastic relaxation. Because the spatial pattern of the viscoelastic deformation has not significantly changed in the present decade, the viscoelastic relaxation is expected to have caused almost the same displacements at these sites before 2014. This supports that the afterslip in the off-Kamaishi region actually caused the relative trench-ward motion of 10 cm/year in three-year average at KAMN before 2014 to cancel the landward motion driven by the viscoelastic relaxation and interseismic backslip (Figure 3b). Furthermore, the temporal evolution of KAMN's movement (Figure 2a) confirms that the afterslip in that region had decayed sufficiently in 3 years. After the decay of the afterslip, the viscoelastic response and interplate coupling became dominant for the crustal deformation around KAMN, similar to the case at neighboring GNSS-A sites (Figures 3b).

To reproduce the difference in average displacement rate of about 10 cm/year between KAMN and KAMS before 2014, afterslip in the northern region outside the coseismic rupture with an average displacement rate on the order of meters per year is required (see Additional file 1: Text S2 for detail). However, the slip magnitude depends on the afterslip distribution, which cannot be geodetically constrained. With the tsunami-derived shallow slip in the off-Kamaishi area taken into account, the afterslip would not have reached the trench at 39 °N (Figure 1b).

In contrast to the off-Miyagi region, rapid trench-ward movements were observed at FUKU and CHOS in the southern region (< 37.5 °N) especially in the first 1–2 years after the Tohoku-oki earthquake (Figures 2e–2f). The trench-ward motion became much smaller after 2013 (Figures 2e–2f). Almost no significant horizontal movement was found at G17, located on the trench side of FUKU, despite the low positioning accuracy due to instrumental malfunction (< 5–6 cm/year for three-year average displacement rate; see Additional file 1: Text S1 for detail).

For the horizontal movement, it is reasonable to assume that the afterslip caused the trench-ward motion with rapid decay of 1–2 years, as shown in the most postseismic models (Sun and Wang, 2015; Iinuma et al., 2016; Freed et al., 2017; Agata et al., 2019). Actually, it had been indicated that viscoelastic deformation cannot cause significant motion at FUKU in some finite element models (Sun et al., 2014; Freed et al., 2017), which used the coseismic input based on the geodetic inversion with a single peak beneath FUKU, such as the model by Iinuma et al. (2012) (Figure 1b). Therefore, such models require to reproduce both the horizontal and vertical motion by only the afterslip. It led to the assumption of the strong afterslip in the shallow portion to explain the rapid subsidence observed at FUKU.

However, subsidence at FUKU continued at almost a constant rate of about 4 cm/year, even after 2014 when the trench-ward movement had almost ceased. This result is against the models which try to explain the most parts of both trench-ward motion and subsidence with a shallow afterslip. A single afterslip cannot cause a persistent subsidence without significant trench-ward movement at FUKU and G17, because of the low dip angle of the plate boundary (see Additional file 1: Text S3 for

This is a non-peer reviewed preprint submitted to EarthArXiv.

detail). Therefore, we should assume another input for the viscoelastic deformation rather than the geodetic inversion model to reproduce the persistent subsidence at FUKU.

Agata et al. (2019) used a coseismic input derived from an earthquake cycle simulation (Nakata et al., 2016), which incorporates an additional peak of coseismic rupture near the trench at 37 °N. Although the source has not reproduced the coseismic seafloor uplift observed at FUKU (Sato et al., 2011), it can provide a practical exercise. Their viscoelastic finite element model demonstrated sufficient subsidence at FUKU. According to the comparisons of the numerical examples of viscoelastic deformation to the coseismic slip distribution, as illustrated in Figure 6 of Sun and Wang (2015), the hinge line of horizontal deformation and the peak of viscoelastic subsidence were located above the downdip side of the major slip. For this reason, the coseismic slip near the trench caused the subsidence at FUKU in the model of Agata et al. (2019). The tsunami-derived coseismic slip distribution in the off-Fukushima region (Satake et al., 2013) has two peaks in the along-dip direction (Figure 1b). Based on the postseismic

This is a non-peer reviewed preprint submitted to EarthArXiv.

model of Agata et al. (2019), the viscoelastic relaxation driven by the shallower coseismic slip can cause long-term subsidence at FUKU (red arrows in Figure 3b).

The discussion above suggests that the tsunami-derived shallow coseismic slip should be adopted in the viscoelastic relaxation model to reasonably explain the spatiotemporal variation of seafloor deformation. In this case, both the viscoelastic relaxation and possible interseismic backslip are predicted to simultaneously cause landward motion at G17 (red and yellow arrows in Figure 3b, respectively). However, it cannot be well detected because of low accuracy at G17. The data is consistent for both cases where G17 actually moves toward the land and where the landward motion is canceled or weaken by remaining afterslip. Therefore, the data cannot constrain the degrees of contribution of viscoelastic response or afterslip to slight trench-ward motion at FUKU in 2014–2017.

In any cases, we can consider that the trench-ward movements at FUKU and CHOS for the first 1–2 years were mainly caused by afterslip in the southern region (purple arrows in Figure 3b). Although we cannot constrain and estimate the spread of southern afterslip region because of low spatial density of geodetic observation site at

This is a non-peer reviewed preprint submitted to EarthArXiv.

that time, annual-scale afterslip was a dominant deformation source in the southern region except for the vertical component at FUKU. Recalling the tsunami-derived rupture distribution at 37 °N, for reproducing the trench-ward motion at FUKU, it might be reasonable to put the afterslip on the fault between the two peaks of the coseismic slip (Figure 1b) rather than putting strong afterslip patches only in far south of FUKU (< 37 °N) as the forward slip model shown by Agata et al. (2019).

Considering that the afterslip occurs on the fault with aseismic frictional property, the assumed afterslip regions on the northern and southern sides of the main rupture are considered to have behaved as barriers to rupture propagation. It is plausible that the shallow tsunamigenic slip in the off-Kamaishi and off-Fukushima areas (Satake et al., 2013) additionally loaded stress on the downdip side and triggered afterslip. The northern afterslip occurred between major earthquakes, i.e., the 1968 Tokachi-oki earthquake ($M_w$ 8.3), the 1994 offshore Sanriku earthquake ($M_w$ 7.7) (Nagai et al., 2001), the 1896 Meiji Sanriku tsunami earthquake ($M_w$ 8.1) (Satake et al., 2017), and the 2011 Tohoku-oki earthquake. The gap between major earthquakes is characterized by relatively low seismicity (Mochizuki et al., 2005), including repeating earthquakes

(Uchida and Matsuzawa, 2013; Igarashi, 2020). Slow earthquake activity has been reported in this area (Nishikawa et al., 2019) as well. Although the northern and along-dip extensions cannot be resolved due to the absence of geodetic instruments, these features are consistent with the aseismic frictional property. In the off-Fukushima region, postseismic movements larger than the main slip were observed for the 2008 and 2010 Fukushima-ken-oki earthquakes ($M_\mathrm{j}$ 6.9 and $M_\mathrm{j}$ 6.7, respectively) (Suito et al., 2011). It is possible that the proposed afterslip in the off-Fukushima region following the Tohoku-oki earthquake occurred in a region near the former afterslip.

## 5 Conclusions

Based on the GNSS-A observations and the above interpretations, the slip behaviors in the northern and southern areas can be summarized as follows. (1) Afterslip occurred in the northern and southern regions outside the main rupture at depths near the hypocenter, which is consistent with the shallower tsunamigenic slip inducing stress on the downdip aseismic faults. It is plausible that these aseismic afterslip regions stopped the north-south rupture propagation. (2) By at least 2014, the afterslip in the off-Kamaishi, off-Fukushima, and off-Choshi regions had almost decayed, though there is less evidence for off-Fukushima region because of less information for determining the viscoelastic deformation patterns. (3) Shallow tsunamigenic slip in the south was captured by postseismic seafloor geodesy as a subsequent viscoelastic deformation that caused persistent seafloor subsidence. Additionally, the GNSS-A results indicate that the long-term viscoelastic relaxation process is currently in progress and is dominant in the off-Miyagi and off-Kamaishi regions. It also plays an important role in the off-Fukushima region, although its contribution cannot be well resolved. These long-term behaviors should be investigated by continuing and expanding seafloor geodetic observations.

# Declarations

### Ethics approval and consent to participate

Not applicable

### Consent for publication

Not applicable

#### List of abbreviations

CMT: Centroid Moment Tensor, GNSS: Global Navigation Satellite

This is a non-peer reviewed preprint submitted to EarthArXiv.

System, GNSS-A: GNSS – acoustic ranging combined seafloor positioning system, JCG: Japan Coast Guard, TU: Tohoku University

## Availability of data and materials

The dataset generated during this study are available at Zenodo (Watanabe et al., 2021c). The GNSS-A analysis software "GARPOS v1.0.0" is available at Zenodo (Watanabe et al., 2021d). The GNSS-A data is available at Zenodo (Watanabe et al., 2021a; b). The daily coordinates of terrestrial GNSS sites were provided by the Geospatial Information Authority of Japan (http://terras.gsi.go.jp) (Nakagawa et al., 2019). The contours for some earthquakes were obtained from the website created by N. Uchida (https://www.aob.gp.tohoku.ac.jp/~uchida/page_3_asp-e.html). The depths of the upper interface of the subducting Pacific plate were obtained from the website created by F. Hirose (https://www.mri-jma.go.jp/Dep/sei/fhirose/plate/en.PlateData.html). The CMT solutions provided by the Japan Meteorological Agency are available at

This is a non-peer reviewed preprint submitted to EarthArXiv.

https://www.data.jma.go.jp/svd/eqev/data/bulletin/index_e.html. Some figures were prepared using Generic Mapping Tools (https://www.generic-mapping-tools.org/).

## Competing interests

Authors declare that they have no competing interests.

## Funding

This study was supported by the Japan Coast Guard (SW, TI, YN) and the University of Tokyo Excellent Young Researcher project (YY).

## Authors' contributions

Conceptualization: SW, TI, YY

Methodology: SW, TI, YN, YY

Software: SW

Formal analysis: SW, YN

Data curation: SW, YN

Investigation: SW, TI, YN, YY

Validation: SW

This is a non-peer reviewed preprint submitted to EarthArXiv.

Visualization: SW

Writing – original draft: SW

Writing – review & editing: SW, TI, YN, YY

**Acknowledgements**

We would like to thank Motoyuki Kido of the Tohoku University for allowing us to use their seafloor geodetic instruments, i.e., G08, G10, G12, G14 and G17. In-situ observations were performed by the survey vessels operated by the Japan Coast Guard.

## References

Agata R, Barbot SD, Fujita K, Hyodo M, Iinuma T, Nakata R, Ichimura T, Hori T (2019) Rapid mantle flow with power-law creep explains deformation after the 2011 Tohoku mega-quake. *Nat Commun* 10:1385. doi:10.1038/s41467-019-08984-7

Altamimi Z, Rebischung P, Métivier L, Collilieux X (2016) ITRF2014: A new release of the International Terrestrial Reference Frame modeling nonlinear station motions. *J Geophys Res Solid Earth* 121:6109–6131. doi:10.1002/2016JB013098

Altamimi Z, Métivier L, Rebischung P, Rouby H, Collilieux X (2017) ITRF2014 plate

This is a non-peer reviewed preprint submitted to EarthArXiv.

motion model. *Geophys J Int* 209:1906–1912. doi: 10.1093/gji/ggx136

Argus DF, Gordon RG, DeMets C (2011) Geologically current motion of 56 plates relative to the no-net-rotation reference frame. *Geochem Geophys Geosyst*, 12:Q11001. doi:10.1029/2011GC003751

Freed AM, Hashima A, Becker TW, Okaya DA, Sato H, Hatanaka Y (2017) Resolving depth-dependent subduction zone viscosity and afterslip from postseismic displacements following the 2011 Tohoku-Oki, Japan earthquake. *Earth Planet Sci Lett* 459:279–290. doi:10.1016/j.epsl.2016.11.040

Fujita M, Ishikawa T, Mochizuki M, Sato M, Toyama S, Katayama M, Kawai K, Matsumoto Y, Yabuki T, Asada A Colombo OL (2006) GPS/acoustic seafloor geodetic observation: method of data analysis and its application. *Earth Planets Space* 58:265–275. doi:10.1186/BF03351923

Fujiwara S, Tobita M, Ozawa S (2021) Spatiotemporal Functional Modeling of Postseismic Deformation After the 2011 Tohoku-Oki Earthquake. *Res Sq*. doi:10.21203/rs.3.rs-423959/v1

Fujiwara T, Kodaira S, No T, Kaiho Y, Takahashi N, Kaneda Y (2011) The 2011 Tohoku-

Oki earthquake: displacement reaching the trench axis. *Science* 334:1240, doi:1240.10.1126/science.1211554

Honsho C, Kido M, Tomita F, Uchida N (2019) Offshore postseismic deformation of the 2011 Tohoku earthquake revisited: Application of an improved GPS-acoustic positioning method considering horizontal gradient of sound speed structure. *J Geophys Res Solid Earth* 124:5990–6009. doi:10.1029/2018JB017135

Igarashi T (2020) Catalog of small repeating earthquakes for the Japanese Islands. *Earth Planets Space* 72:73. doi:10.1186/s40623-020-01205-2

Iinuma T, Hino R, Kido M, Inazu D, Osada Y, Ito Y, Ohzono M, Tsushima H, Suzuki S, Fujimoto H, Miura S (2012) Coseismic slip distribution of the 2011 off the Pacific Coast of Tohoku Earthquake (M9.0) refined by means of seafloor geodetic data. *J Geophys Res* 117:B07409. doi:10.1029/2012JB009186

Iinuma T, Hino R, Uchida N, Nakamura W, Kido M, Osada Y, Miura S (2016) Seafloor observations indicate spatial separation of coseismic and postseismic slips in the 2011 Tohoku earthquake. *Nat Commun* 7:13506. doi:10.1038/ncomms13506

Ishikawa T, Yokota Y, Watanabe S, Nakamura Y (2020) History of on-board equipment improvement for GNSS-A observation with focus on observation frequency. *Front Earth Sci* 8:150. doi:10.3389/feart.2020.00150

Kido M, Fujimoto H, Hino R, Ohta Y, Osada Y, Iinuma T, Azuma R, Wada I, Miura S, Suzuki S, Tomita F, Imano M (2015) Progress in the project for development of GPS/Acoustic technique over the last 4 years. In: Hashimoto M (ed) *International Symposium on Geodesy for Earthquake and Natural Hazards (GENAH)*. Springer, pp 3–10. doi:10.1007/1345_2015_127

Kido M, Osada Y, Fujimoto H, Hino R, Ito Y (2011) Trench-normal variation in observed seafloor displacements associated with the 2011 Tohoku-Oki earthquake. *Geophys Res Lett* 38:L24303. doi:10.1029/2011GL050057

Mochizuki K, Nakamura M, Kasahara J, Hino R, Nishino M, Kuwano A, Nakamura Y, Yamada T, Shinohara M, Sato T, Moghaddam PP, Kanazawa T (2005) Intense PP reflection beneath the aseismic forearc slope of the Japan Trench subduction zone and its implication of aseismic slip subduction. *J Geophys Res* 110:B01302. doi: 10.1029/2003JB002892

Nagai, R., Kikuchi, M., Yamanaka, Y. (2001) Comparative study on the source processes

This is a non-peer reviewed preprint submitted to EarthArXiv.

of recurrent large earthquakes in Sanriku-oki Region: The 1968 Tokachi-oki earthquake and the 1994 Sanriku-oki earthquake. *Zisin(2)*, 54, 267-280. doi:10.4294/zisin1948.54.2_267

Nakata R, Hori T, Hyodo M, Ariyoshi K (2016) Possible scenarios for occurrence of M～7 interplate earthquakes prior to and following the 2011 Tohoku-Oki earthquake based on numerical simulation. *Sci Rep* 6:25704. doi:10.1038/srep25704

Nakagawa H, Toyofuku T, Kotani K, Miyahara B, Iwashita C, Kawamoto S, Hatanaka Y, Munekane H, Ishimoto M, Yutsudo T, Ishikura N, Sugawara Y (2009) Development and validation of GEONET new analysis strategy (Version 4). *J Geographical Survey Inst* 118:1–8.

Nishikawa T, Matsuzawa T, Ohta K, Uchida N, Nishimura T, Ide S (2019) The slow earthquake spectrum in the Japan Trench illuminated by the S-net seafloor observatories. *Science* 365:808–813. doi:10.1126/science.aax5618

Okada Y (1992) Internal deformation due to shear and tensile faults in a half-space. *Bull Seism Soc Am* 82:1018-1040

Ozawa S, Nishimura T, Munekane H, Suito H, Kobayashi T, Tobita M, Imakiire T (2012)

This is a non-peer reviewed preprint submitted to EarthArXiv.

Preceding, coseismic, and postseismic slips of the 2011 Tohoku earthquake, Japan. *J Geophys Res* 117:B07404. doi:10.1029/2011JB009120

Satake K, Fujii Y, Harada T, Namegaya Y (2013) Time and space distribution of coseismic slip of the 2011 Tohoku earthquake as inferred from tsunami waveform data. *Bull Seismol Soc Am* 103:1473–1492. doi:10.1785/0120120122

Satake K, Fujii Y, Yamaki S (2017) Different depths of near-trench slips of the 1896 Sanriku and 2011 Tohoku earthquakes. *Geosci Lett* 4:33. doi:10.1186/s40562-017-0099-y

Sato M, Fujita M, Matsumoto Y, Ishikawa T, Saito H, Mochizuki M, Asada A (2013a) Interplate coupling off northeastern Japan before the 2011 Tohoku-oki earthquake, inferred from seafloor geodetic data. *J Geophys Res* 118:3860–3869. doi:10.1002/jgrb.50275

Sato M, Fujita M, Matsumoto Y, Saito H, Ishikawa T, Asakura T (2013b) Improvement of GPS/acoustic seafloor positioning precision through controlling the ship’s track line. *J Geod*, 118:1–10. doi:10.1007/s00190-013-0649-9

This is a non-peer reviewed preprint submitted to EarthArXiv.

Sato M, Ishikawa T, Ujihara N, Yoshida S, Fujita M, Mochizuki M, Asada A (2011) Displacement above the hypocenter of the 2011 Tohoku-oki earthquake. *Science* 332:1395. doi:10.1126/science.1207401

Suito H, Nishimura T, Tobita M, Imakiire T, Ozawa S (2011) Interplate fault slip along the Japan Trench before the occurrence of the 2011 off the Pacific coast of Tohoku Earthquake as inferred from GPS data. *Earth Planets Space* 63:615–619. doi:10.5047/eps.2011.06.053

Sun T, Wang K (2015) Viscoelastic relaxation following subduction earthquakes and its effects on afterslip determination. *J Geophys Res* 120:1329–1344. doi:10.1002/2014JB011707

Sun T, Wang K, Fujiwara T, Kodaira S, He J (2017) Large fault slip peaking at trench in the 2011 Tohoku-oki earthquake. *Nat Commun* 8:14044. doi:10.1038/ncomms14044

Sun T, Wang K, Iinuma T, Hino R, He J, Fujimoto H, Kido M, Osada Y, Miura S, Ohta Y, Hu Y (2014) Prevalence of viscoelastic relaxation after the 2011 Tohoku-oki earthquake. *Nature* 514:84–87. doi:10.1038/nature13778

Tobita M (2016) Combined logarithmic and exponential function model for fitting postseismic GNSS time series after 2011 Tohoku-Oki earthquake. *Earth Planets Space* 68:41. doi:10.1186/s40623-016-0422-4

Tomita F, Kido M, Ohta Y, Iinuma T, Hino R (2017) Along-trench variation in seafloor displacements after the 2011 Tohoku earthquake. *Sci Adv* 3(7):e1700113. doi:10.1126/sciadv.1700113

Uchida N, Matsuzawa T (2013) Pre- and postseismic slow slip surrounding the 2011 Tohoku-oki earthquake rupture. *Earth Planet Sci Lett* 374:81–91. doi:10.1016/j.epsl.2013.05.021

Wang K, Hu Y, He J (2012) Deformation cycles of subduction earthquake in a viscoelastic Earth. *Nature* 484:327–332. doi:10.1038/nature11032

Wang K, Sun T, Brown L, Hino R, Tomita F, Kido M, Iinuma T, Kodaira S, Fujiwara T (2018) Learning from crustal deformation associated with M9 2011 Tohoku-oki earthquake. *Geosphere* 14:552–571. doi:10.1130/GES01531.1

Watanabe S, Ishikawa T, Nakamura Y, Yokota Y (2021a) GNSS-A data obtained at the sites along the Japan Trench before the 2011 Tohoku-oki earthquake (Version 1.0.0). *Zenodo*. doi:10.5281/zenodo.4528990

This is a non-peer reviewed preprint submitted to EarthArXiv.

Watanabe S, Ishikawa T, Nakamura Y, Yokota Y (2021b) GNSS-A data obtained at the sites along the Japan Trench from March 2011 to June 2020 (Version 1.0.0). *Zenodo*. doi:10.5281/zenodo.4529008

Watanabe S, Ishikawa T, Nakamura Y, Yokota Y (2021c) Time series of seafloor displacement at GNSS-A sites along the Japan Trench: from March 2011 to June 2020 and before the 2011 Tohoku-oki earthquake (Version 1.0.0). *Zenodo*. doi:10.5281/zenodo.4628550

Watanabe S, Ishikawa T, Yokota Y, Nakamura Y (2020) GARPOS: Analysis Software for the GNSS-A seafloor positioning with simultaneous estimation of sound speed structure. *Front Earth Sci* 8:597532. doi:10.3389/feart.2020.597532

Watanabe S, Ishikawa T, Yokota Y, Nakamura Y (2021d) GARPOS: Analysis tool for GNSS-Acoustic seafloor positioning (Version 1.0.0). *Zenodo*. doi:10.5281/zenodo.4522027

Watanabe S, Sato M, Fujita M, Ishikawa T, Yokota Y, Ujihara N, Asada A (2014) Evidence of viscoelastic deformation following the 2011 Tohoku-oki earthquake revealed from seafloor geodetic observation. *Geophys Res Lett* 41:5789–5796.

This is a non-peer reviewed preprint submitted to EarthArXiv.

doi:10.1002/2014GL061134

Yamanaka Y, Kikuchi M (2004) Asperity map along the subduction zone in northeastern Japan inferred from regional seismic data. *J Geophys Res* 109:B07307. doi: 10.1029/2003JB002683

This is a non-peer reviewed preprint submitted to EarthArXiv.

**Figure legends**

**Figure 1**. **Seafloor motion derived from GNSS-A observations.** Average horizontal and vertical velocities for (**a**) pre-seismic period, and three-year cumulative displacements for (**b**) 2011–2014, (**c**) 2014–2017, and (**d**) 2017–2020 are indicated as black arrows and open rectangles, respectively. Terrestrial GNSS velocities or cumulative displacements were extracted from the F3 solution of the GEONET sites (Nakagawa et al., 2009). Onshore velocities during 2007–2011 are shown in (**a**). Purple patches indicate possible afterslip regions, but there is little or no resolution for the spread. Brown contours and colored tiles indicate geodetically derived (Iinuma et al., 2012) and tsunami-derived (Satake et al., 2013) coseismic slip distributions of the 2011 Tohoku-oki earthquake, respectively. Green circles denote repeating earthquakes that occurred in each period (Igarashi, 2020). CMT solutions for the use of displacement correction are shown in each panel. Navy and blue lines indicate 2-m and 4-m slip contours of historical earthquakes in the northern area (Nagai et al., 2001). Green

rectangles indicate patches with a slip of 20 m for the 1896 tsunami earthquake (Satake et al., 2017).

**Figure 2. Time series of postseismic seafloor displacement.** Displacements with respect to the Okhotsk plate of NNR-MORVEL56 model (Argus et al., 2011) are shown (black circles). Fitted logarithmic curves are shown as the solid lines. The 95 % confidence intervals for curve fittings are shown as shaded areas. Results provided by Honsho et al. (2019) for (g)–(k) are indicated as brown squares.

**Figure 3**. **Schematic diagram of deformation sources beneath the seafloor.** (**a**) Slips on the plate interface. Purple, red, and orange regions indicate possible afterslip region and geodetically derived (Iinuma et al., 2012) and tsunami-derived (Satake et al., 2013) coseismic slip areas of the 2011 Tohoku-oki earthquake, respectively. Blue circles and bars indicate the locations of GNSS-A sites and their projections to the plate interface, respectively. Black rectangles show the locations for cross sections illustrated in subsequent panels. Note that there is little or no information for the spread of afterslip regions. (**b**) Cross sections for each region with one of possible qualitative explanations for the contributions of each deformation source to the motion at GNSS-A sites. Black,

This is a non-peer reviewed preprint submitted to EarthArXiv.

red, purple, and yellow arrows indicate the observed motion and components due to viscoelastic relaxation, afterslip, and interplate coupling, respectively.

**Table legends**

**Table 1. Summary of previously proposed postseismic deformation models.** Models with (1) referencing the seafloor geodetic data, (2) incorporating the afterslip dislocation models, (3) modeling the subducting cold slab, and (4) calculating the viscoelastic deformation in wider area than a latitude range of 37–39 °N, are shown.

**Table 2. Displacements with respect to the Okhotsk plate from the fitted curves with 95% confidence intervals.**

(**a**) Average velocity before 2011

(**b**) Three-year cumulative displacement from Apr. 2011 to Apr. 2014.

(**c**) Three-year cumulative displacement from Apr. 2014 to Apr. 2017.

(**d**) Three-year cumulative displacement from Apr. 2017 to Apr. 2020.z

**Supplementary Information**

**Additional file 1**

Figure S1 shows schematic diagrams of the GNSS-A observation operated by the Japan

This is a non-peer reviewed preprint submitted to EarthArXiv.

Coast Guard. Figures S2 shows the time series of preseismic seafloor displacements with respect to the Okhotsk plate. Text S1 describes the validations for the GNSS-A results obtained at G17, which has lower precision than the other sites. Figure S3 shows the actual track lines during the GNSS-A campaign observations at G17, which is referenced in Text S1. Texts S2 and S3 discuss the validity or invalidity of afterslip contributions to the GNSS-A data in the northern and southern regions, respectively. Figures S4 and S5 show the contributions of interplate dislocations to the GNSS-A sites in the northern and southern regions, respectively. Table S1 shows the reference locations of the GNSS-A sites.

**Table 1. Summary of previously proposed postseismic deformation models.** Models with (1) referencing the seafloor geodetic data, (2) incorporating the afterslip dislocation models, (3) modeling the subducting cold slab, and (4) calculating the viscoelastic deformation in wider area than a latitude range of 37–39 °N, are shown.

| Reference | Rheology model | Coseismic input (source) | Afterslip model | Approx. period |
|---|---|---|---|---|
| Sun et al. (2014) | Burgers model | Geodetic inversion (Iinuma et al. 2012) | Modified from Ozawa et al. (2012) with trial-and-error | 3 year |
| Sun & Wang (2015) | Same model as Sun et al. (2014) | | Ad hoc shallow patches added to Sun et al. (2014) | 3 year |
| Wang et al. (2018) | Same model as Sun et al. (2014) | | Ad hoc afterslip patches added to Sun & Wang (2015) | 5 years |
| Iinuma et al. (2016) | Same model as Sun et al. (2014) | | Geodetic inversion after removing viscoelastic effect | 0.7 year |
| Freed et al. (2017) | Maxwell model / depth-dependent | Geodetic inversion (self-derived) | Geodetic inversion after removing viscoelastic effect | 3 year |
| Agata et al. (2019) | Power-law / thermally activated | Earthquake simulation (Nakata et al., 2016) | Forward calculation based on rate- & state-dependent friction | 2.8 year |

**Table 2. Displacements with respect to the Okhotsk plate from the fitted curves with 95% confidence intervals.**

(**a**) Average velocity before 2011

| Site | Displacement (cm/year) | | | Variance-covariance ((cm/year)$^2$) | | | |
|---|---|---|---|---|---|---|---|
| | E-ward | N-ward | U-ward | V(E,E) | V(E,N) | V(N,N) | V(U,U) |
| KAMN | -3.5 | 0.4 | 0.1 | 0.40 | 0.12 | 0.67 | 2.61 |
| KAMS | -2.4 | -1.8 | 0.7 | 2.29 | -1.01 | 1.71 | 2.10 |
| MYGI | -4.1 | 2.4 | -2.0 | 0.24 | -0.03 | 0.50 | 0.93 |
| MYGW | -4.5 | 1.2 | -0.2 | 0.22 | -0.19 | 0.23 | 2.06 |
| FUKU | -1.8 | -1.3 | -2.0 | 0.30 | 0.17 | 1.15 | 3.15 |

(**b**) Three-year cumulative displacement from Apr. 2011 to Apr. 2014.

| Site | Displacement (cm) | | | Variance-covariance (cm$^2$) | | | |
|---|---|---|---|---|---|---|---|
| | E-ward | N-ward | U-ward | V(E,E) | V(E,N) | V(N,N) | V(U,U) |
| KAMN | -4.0 | 3.6 | -21.5 | 4.76 | 3.98 | -1.45 | 11.24 |
| KAMS | -32.6 | 14.9 | -16.1 | 18.22 | 12.28 | -6.08 | 16.05 |
| MYGI | -28.2 | 8.4 | -21.4 | 5.35 | 4.99 | 0.46 | 7.34 |
| MYGW | 7.8 | -14.8 | -32.5 | 2.73 | 3.11 | 0.57 | 7.29 |
| FUKU | 60.4 | -41.9 | -42.1 | 3.56 | 5.00 | -1.59 | 8.34 |
| CHOS | 59.8 | -26.1 | 5.3 | 7.60 | 24.06 | 3.73 | 27.44 |

(**c**) Three-year cumulative displacement from Apr. 2014 to Apr. 2017.

| Site | Displacement (cm) | | | Variance-covariance ($cm^2$) | | | |
|---|---|---|---|---|---|---|---|
| | **E-ward** | **N-ward** | **U-ward** | **V(E,E)** | **V(E,N)** | **V(N,N)** | **V(U,U)** |
| KAMN | -17.0 | 4.4 | -5.6 | 0.78 | 0.65 | -0.24 | 1.84 |
| KAMS | -22.0 | 6.8 | -7.0 | 2.56 | 1.73 | -0.86 | 2.26 |
| MYGI | -20.1 | 7.6 | -10.6 | 1.22 | 1.14 | 0.11 | 1.68 |
| MYGW | -3.3 | -2.2 | -8.6 | 0.61 | 0.70 | 0.13 | 1.63 |
| FUKU | 5.7 | -6.8 | -15.5 | 0.61 | 0.86 | -0.27 | 1.44 |
| CHOS | 1.5 | -1.0 | 0.3 | 0.61 | 1.92 | 0.30 | 2.19 |
| TU08 | -25.5 | 10.5 | -3.7 | 10.39 | 6.56 | -5.44 | 15.66 |
| TU10 | -28.0 | 13.2 | -4.9 | 6.41 | 19.65 | -1.75 | 17.88 |
| TU12 | -38.7 | 17.1 | -7.0 | 10.36 | 14.54 | -2.31 | 14.64 |
| TU14 | -21.2 | 7.4 | -12.2 | 1.58 | 1.96 | -0.94 | 3.55 |
| TU17 | 6.7 | -10.4 | -0.5 | 23.65 | 9.54 | 2.44 | 57.68 |

(**d**) Three-year cumulative displacement from Apr. 2017 to Apr. 2020.

| Site | Displacement (cm) | | | Variance-covariance ($cm^2$) | | | |
|---|---|---|---|---|---|---|---|
| | **E-ward** | **N-ward** | **U-ward** | **V(E,E)** | **V(E,N)** | **V(N,N)** | **V(U,U)** |
| KAMN | -20.5 | 5.3 | -3.7 | 1.61 | 1.35 | -0.49 | 3.80 |
| KAMS | -22.3 | 8.1 | -6.5 | 4.78 | 3.22 | -1.59 | 4.21 |
| MYGI | -20.7 | 7.4 | -8.8 | 2.49 | 2.32 | 0.21 | 3.42 |
| MYGW | -7.2 | -0.4 | -6.1 | 1.24 | 1.42 | 0.26 | 3.32 |
| FUKU | -0.1 | -1.1 | -12.4 | 1.20 | 1.70 | -0.54 | 2.82 |
| CHOS | -2.2 | 2.0 | -2.0 | 1.00 | 3.15 | 0.49 | 3.60 |
| TU08 | -18.5 | 10.8 | 4.0 | 15.90 | 10.03 | -8.33 | 23.96 |
| TU10 | -26.0 | 17.5 | 0.5 | 13.18 | 40.40 | -3.59 | 36.77 |
| TU12 | -28.4 | 19.3 | 6.2 | 19.49 | 27.35 | -4.34 | 27.54 |
| TU14 | -18.2 | 7.7 | -6.1 | 2.45 | 3.02 | -1.46 | 5.49 |
| TU17 | -3.6 | -4.2 | 15.4 | 46.94 | 18.92 | 4.84 | 114.47 |

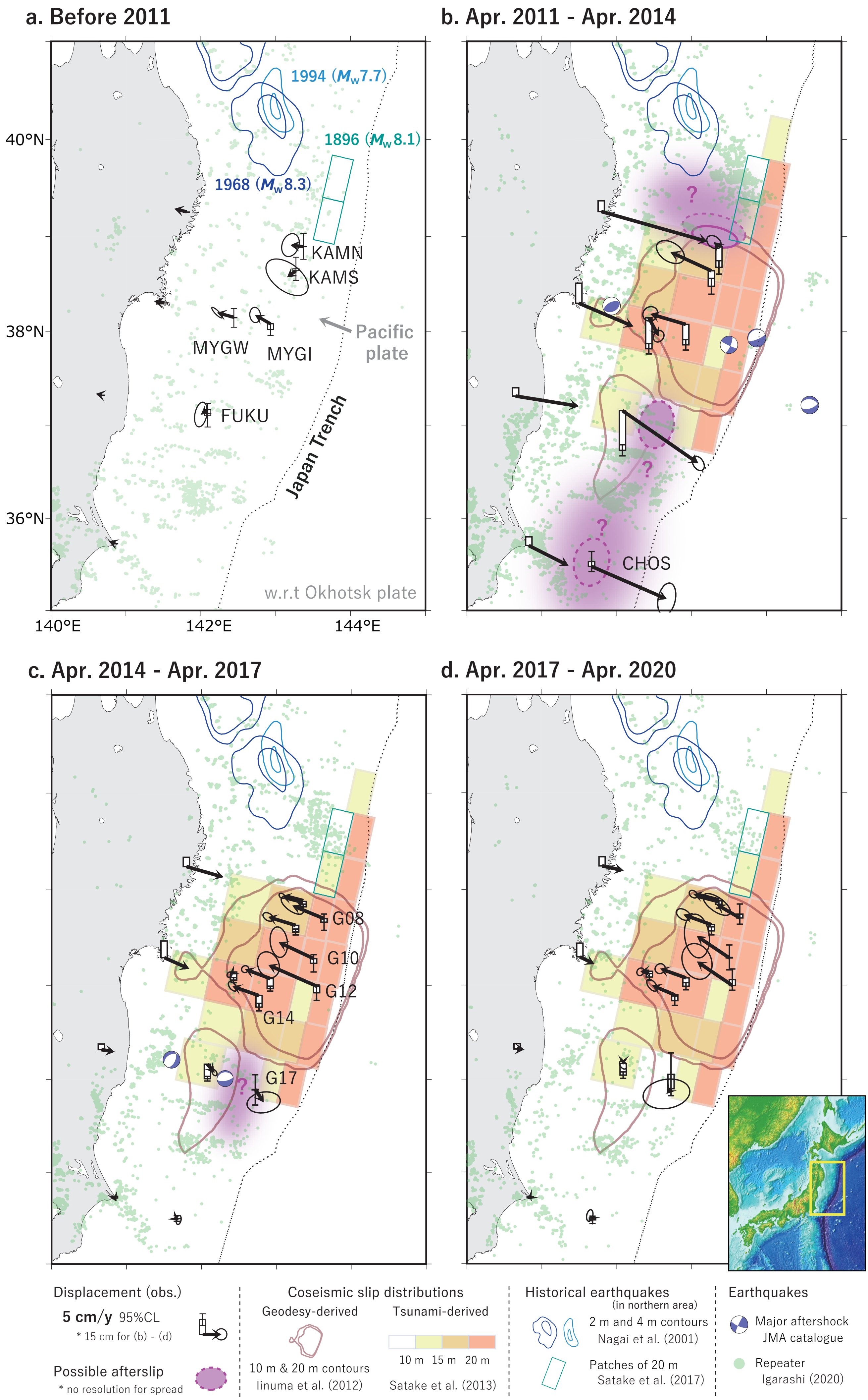

a. Before 2011
b. Apr. 2011 - Apr. 2014
c. Apr. 2014 - Apr. 2017
d. Apr. 2017 - Apr. 2020
1994 ($M_w$7.7)
1896 ($M_w$8.1)
1968 ($M_w$8.3)
40°N
38°N
36°N
140°E
142°E
144°E
KAMN
KAMS
MYGW
MYGI
FUKU
Pacific plate
Japan Trench
w.r.t Okhotsk plate
CHOS
G08
G10
G12
G14
G17
Displacement (obs.)
5 cm/y 95%CL
* 15 cm for (b) - (d)
Possible afterslip
* no resolution for spread
Coseismic slip distributions
Geodesy-derived
10 m & 20 m contours
Iinuma et al. (2012)
Tsunami-derived
10 m 15 m 20 m
Satake et al. (2013)
Historical earthquakes
(in northern area)
2 m and 4 m contours
Nagai et al. (2001)
Patches of 20 m
Satake et al. (2017)
Earthquakes
Major aftershock
JMA catalogue
Repeater
Igarashi (2020)

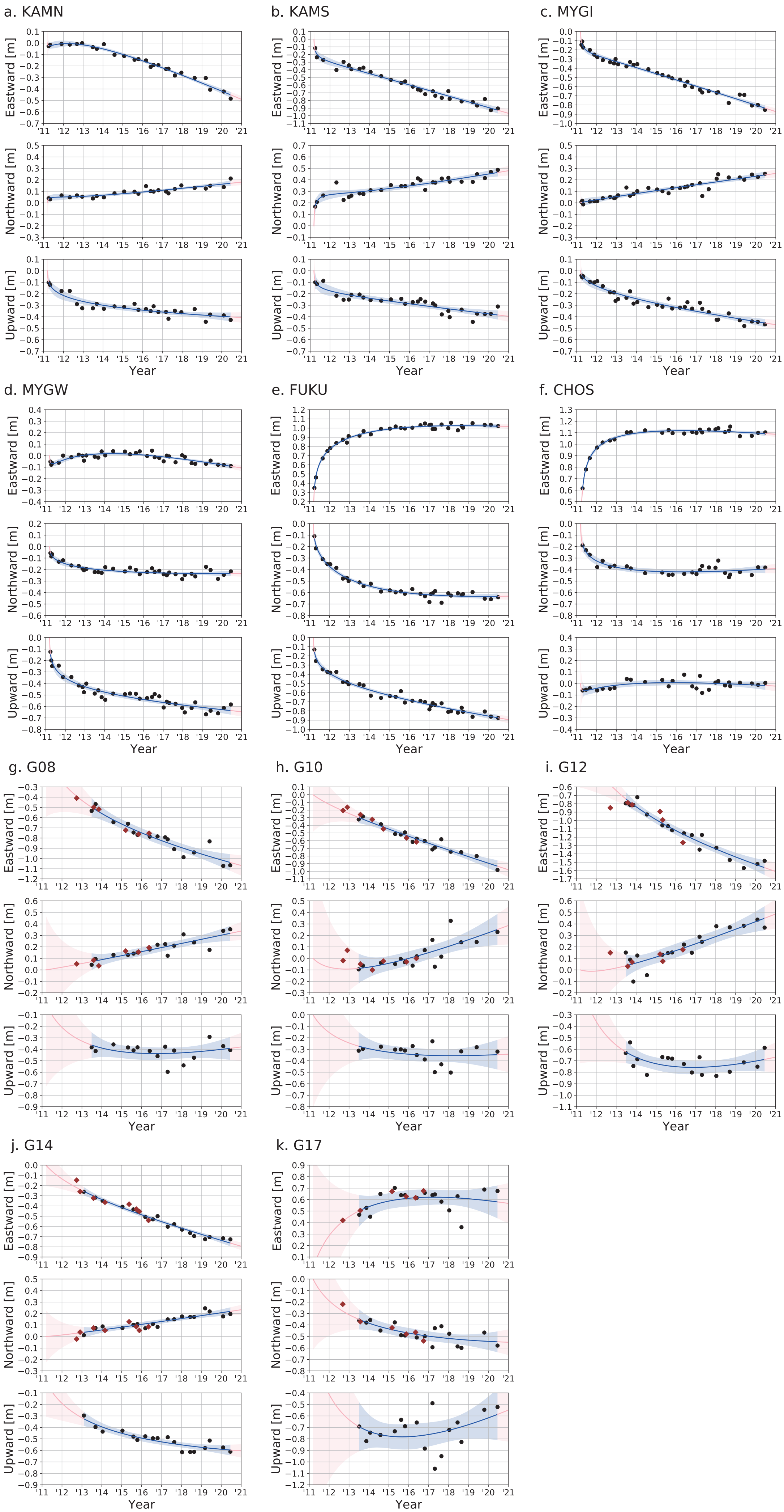
a. KAMN
b. KAMS
c. MYGI
d. MYGW
e. FUKU
f. CHOS
g. G08
h. G10
i. G12
j. G14
k. G17
Eastward [m]
Northward [m]
Upward [m]
Year

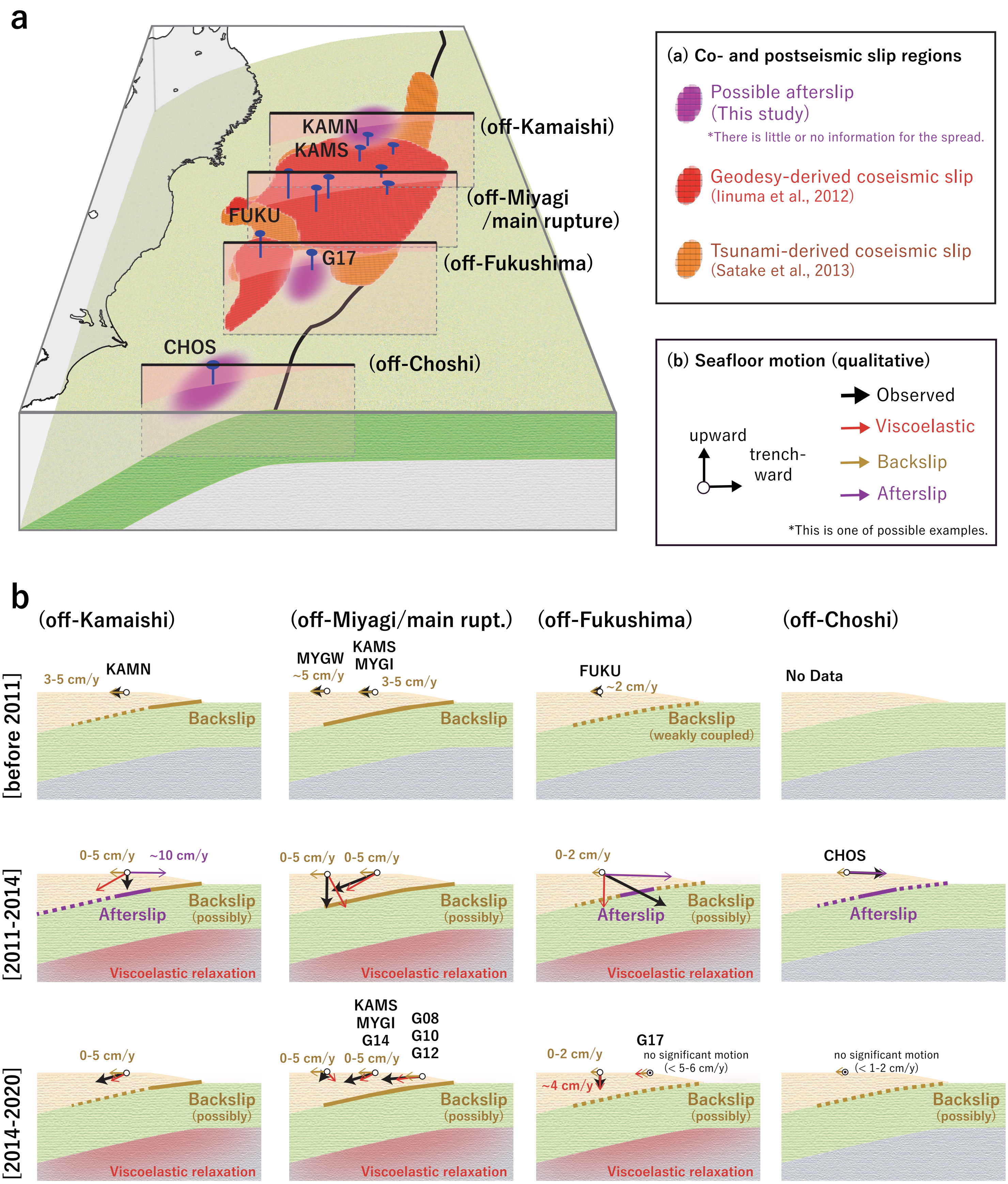

a
KAMN
KAMS
FUKU
G17
CHOS
(off-Kamaishi)
(off-Miyagi /main rupture)
(off-Fukushima)
(off-Choshi)
(a) Co- and postseismic slip regions
Possible afterslip (This study)
*There is little or no information for the spread.
Geodesy-derived coseismic slip (Iinuma et al., 2012)
Tsunami-derived coseismic slip (Satake et al., 2013)
(b) Seafloor motion (qualitative)
upward
trench-ward
Observed
Viscoelastic
Backslip
Afterslip
*This is one of possible examples.
b
(off-Kamaishi)
(off-Miyagi/main rupt.)
(off-Fukushima)
(off-Choshi)
[before 2011]
[2011-2014]
[2014-2020]
3-5 cm/y
KAMN
MYGW
~5 cm/y
KAMS
MYGI
3-5 cm/y
FUKU
~2 cm/y
No Data
Backslip
Backslip (weakly coupled)
0-5 cm/y
~10 cm/y
0-2 cm/y
CHOS
Afterslip
Backslip (possibly)
Viscoelastic relaxation
KAMS
MYGI
G14
G08
G10
G12
G17
no significant motion (< 5-6 cm/y)
no significant motion (< 1-2 cm/y)
~4 cm/y

Additional file 1 for

# Co- and postseismic slip behaviors extracted from decadal seafloor geodesy after the 2011 Tohoku-oki earthquake

S. Watanabe[1], T. Ishikawa[1], Y. Nakamura[1], and Y. Yokota[2]

[1]Hydrographic and Oceanographic Department, Japan Coast Guard

[2]Institute of Industrial Science, University of Tokyo

## Contents



**Overview.**

Figure S1 shows schematic diagrams of the GNSS-A observation operated by the Japan Coast Guard. Figures S2 shows the time series of preseismic seafloor displacements with respect to the Okhotsk plate. Text S1 describes the validations for the GNSS-A results obtained at G17, which has lower precision than the other sites. Figure S3 shows the actual track lines during the GNSS-A campaign observations at G17, which is referenced in Text S1. Texts S2 and S3 discuss the validity or invalidity of afterslip contributions to the GNSS-A data in the northern and southern regions, respectively. Figures S4 and S5 show the contributions of interplate dislocations to the GNSS-A sites in the northern and southern regions, respectively. Table S1 shows the reference locations of the GNSS-A sites.

**Text S1.**

The previous study performed by the TU research group (Honsho et al., 2019) showed an average velocity of approximately 10 cm/year toward the trench at G17 in a period between 2012 and 2016 and is consistent with our results of the period after 2014, which we are discussing in this study. However, the results at G17 indicated a lower positioning precision compared to the other sites. There should be several reasons as follows: Firstly, mirror transponders installed at G17 frequently misrecognized their identification numbers for acoustic ranging, which are necessary to distinguish the transponder that responded to the acoustic signal. Secondly, the on-board systems on some vessels were unable to perform acoustic ranging longer than 10 seconds so that the track line had to be shrunken, until restoration in 2019 (Figure S3). In practice, lack of acoustic data from the outside of the transponder array significantly degrades the positioning accuracy (Nakamura et al., 2021). These errors have also occurred at G12, but G17 seemed to be affected more significantly. The difference between G12 and G17 might be caused by the transponder arrangement or the complexity in the seawater sound speed structure. Although we cannot quantify the positioning accuracy, the results from late 2016 to 2018 tend to contain larger uncertainty than in the other period with wider track line.

**Text S2.**

We examine how interplate afterslip can reproduce the relative trench-ward (ESE-ward) seafloor movements of 10 cm/year at KAMN with respect to KAMS. We calculated the displacements at KAMN and KAMS caused by a dislocation on each 5 km x 5 km subfault placed at intervals of 0.5° in latitude and longitude, in an elastic half-space medium (Okada, 1992). For simplification, strike, dip, and rake angles of the subfaults are fixed to 195°, 13°, and 90°, respectively. The depths of the subfaults are referenced to Nakajima and Hasegawa (2006). Figure S4 shows the subfaults' contributions to the seafloor movements at KAMN and KAMS. The subfaults located beneath and in the northern side of KAMN significantly contribute to the generation of a relative trench-ward motion at KAMN (green region in Figure S4a). Because the surface displacement from a unit slip on a subfault is $O(10^{-3})$, roughly 100 subfaults with a 1 m/year slip can reproduce the relative velocity of 0.1 m/year. This is equivalent to a 50 km x 50 km rectangular fault. There is no resolution for the slip in the white region in Figure S4a, which indicates that our data cannot resolve the afterslip in these regions.

**Text S3.**

We examine the coupling of subsidence and trench-ward (ESE-ward) motion at FUKU caused by interplate afterslip. We calculated the displacements at FUKU caused by a dislocation on each 5 km x 5 km subfault placed at intervals of 0.5° in latitude and longitude, in an elastic half-space medium (Okada, 1992). For simplification, strike, dip, and rake angles of subfault are fixed to 200°, 13°, and 90°, respectively. The depths of the subfaults are referenced to Nakajima and Hasegawa (2006). Figure S5 shows the subfaults' contributions to the seafloor movements at FUKU. Almost all of the subfaults causing subsidence at FUKU (blue region in Figure S5b) simultaneously cause significant trench-ward motion (green region in Figure S5a).

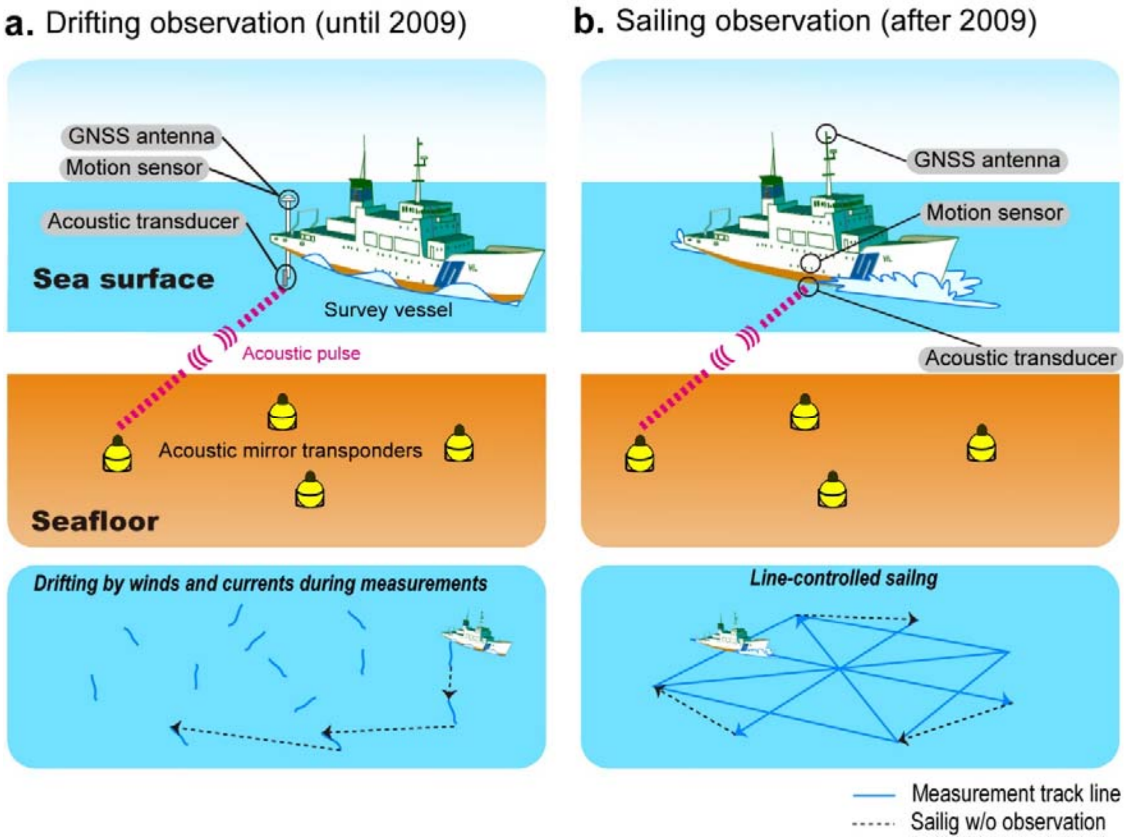


**Figure S1.** Schematic diagrams of the GNSS-A observation. Observation configurations for (a) drifting and (b) sailing systems are shown.

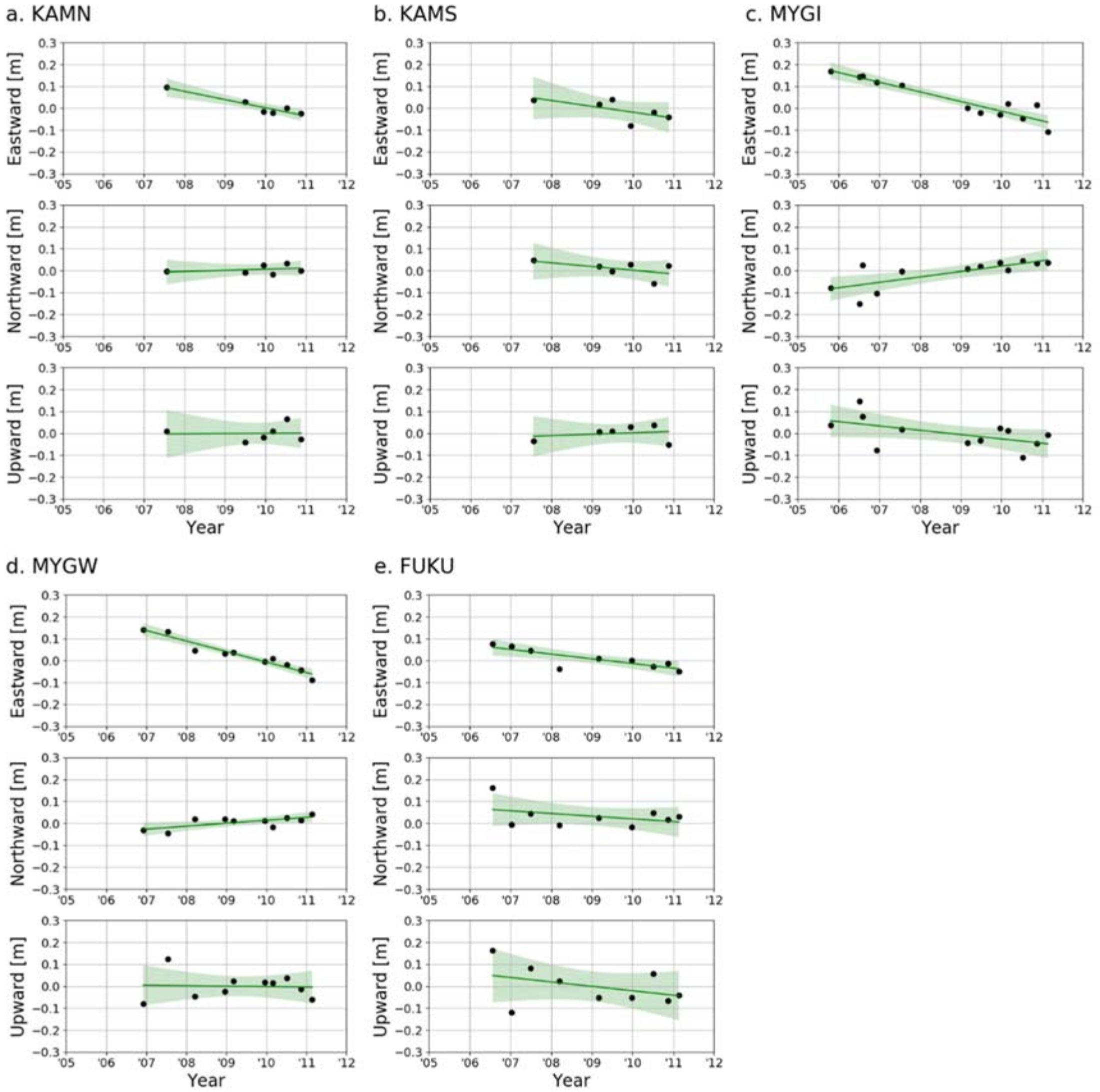


**Figure S2.** Time series of preseismic seafloor displacement. Displacements with respect to the Okhotsk plate of NNR-MORVEL56 model (Argus et al., 2011) are shown (black circles). Average velocities and their 95 % confidence intervals are shown as solid lines and shaded areas, respectively.

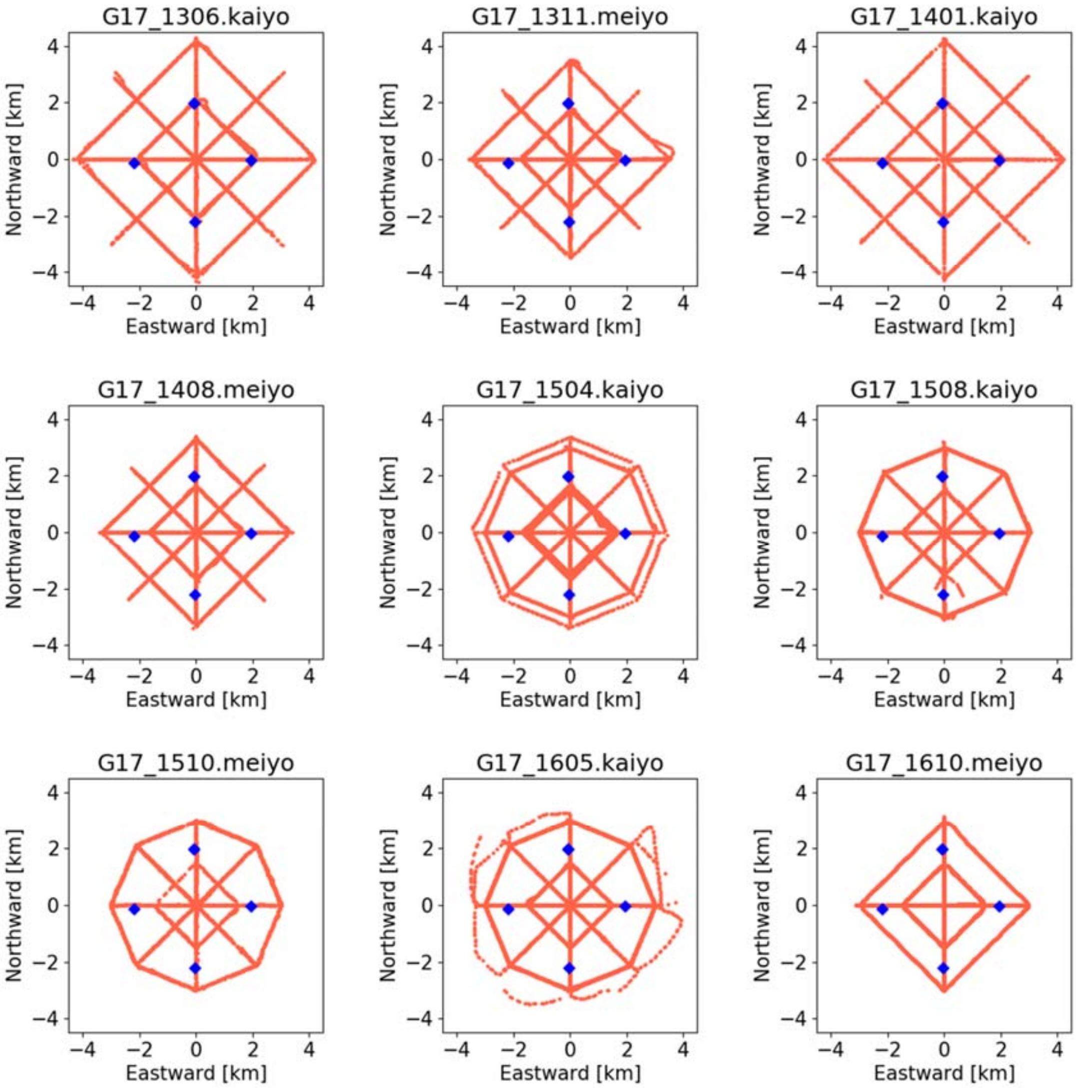


**Figure S3.** Track lines at G17. Orange dots and blue squares indicate the positions of the surface transducer for each acoustic data and the seafloor transponders, respectively. Titles on each panel shows the 4-digit year-month and the name of the used vessel.

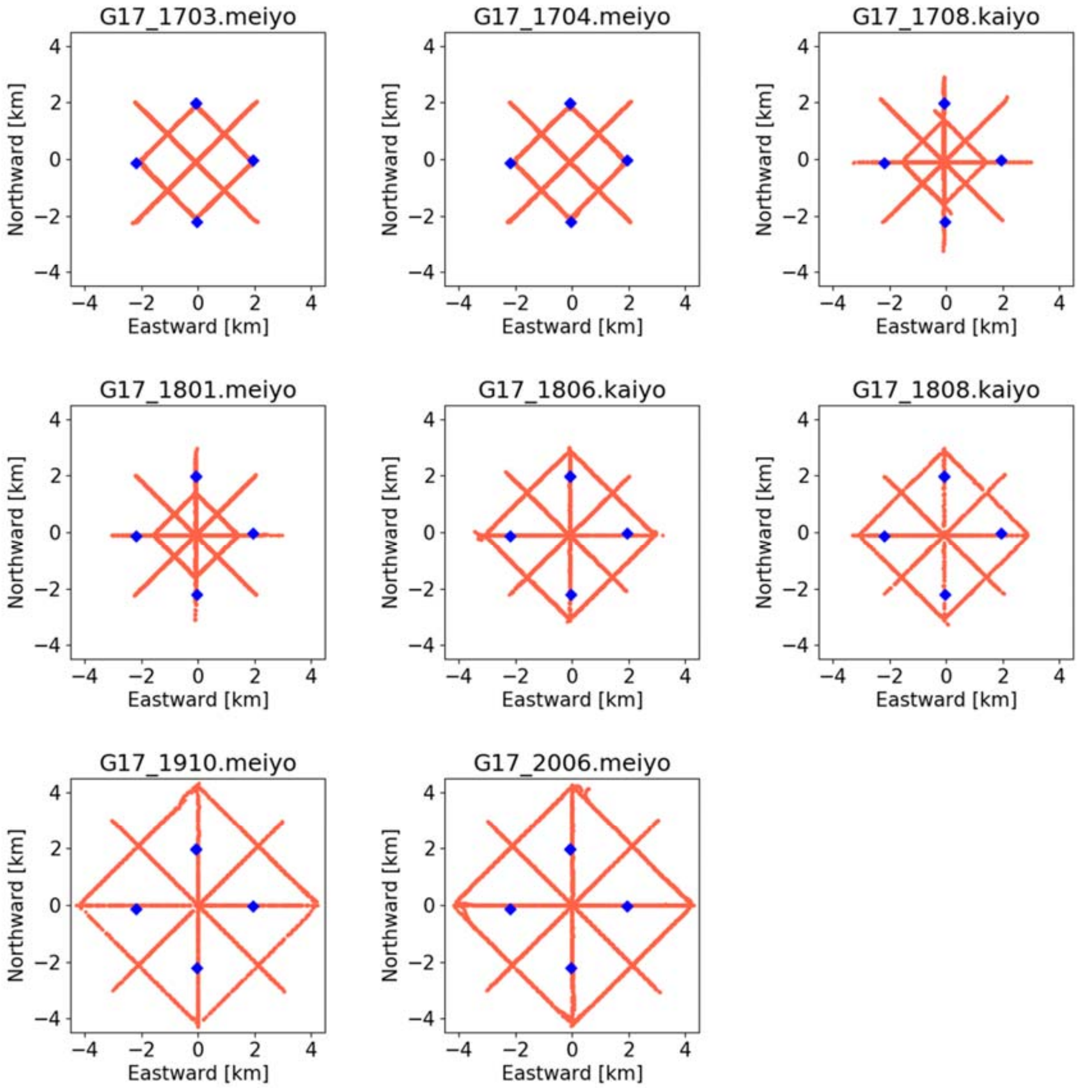


**Figure S3.** Track lines at G17 (continued).

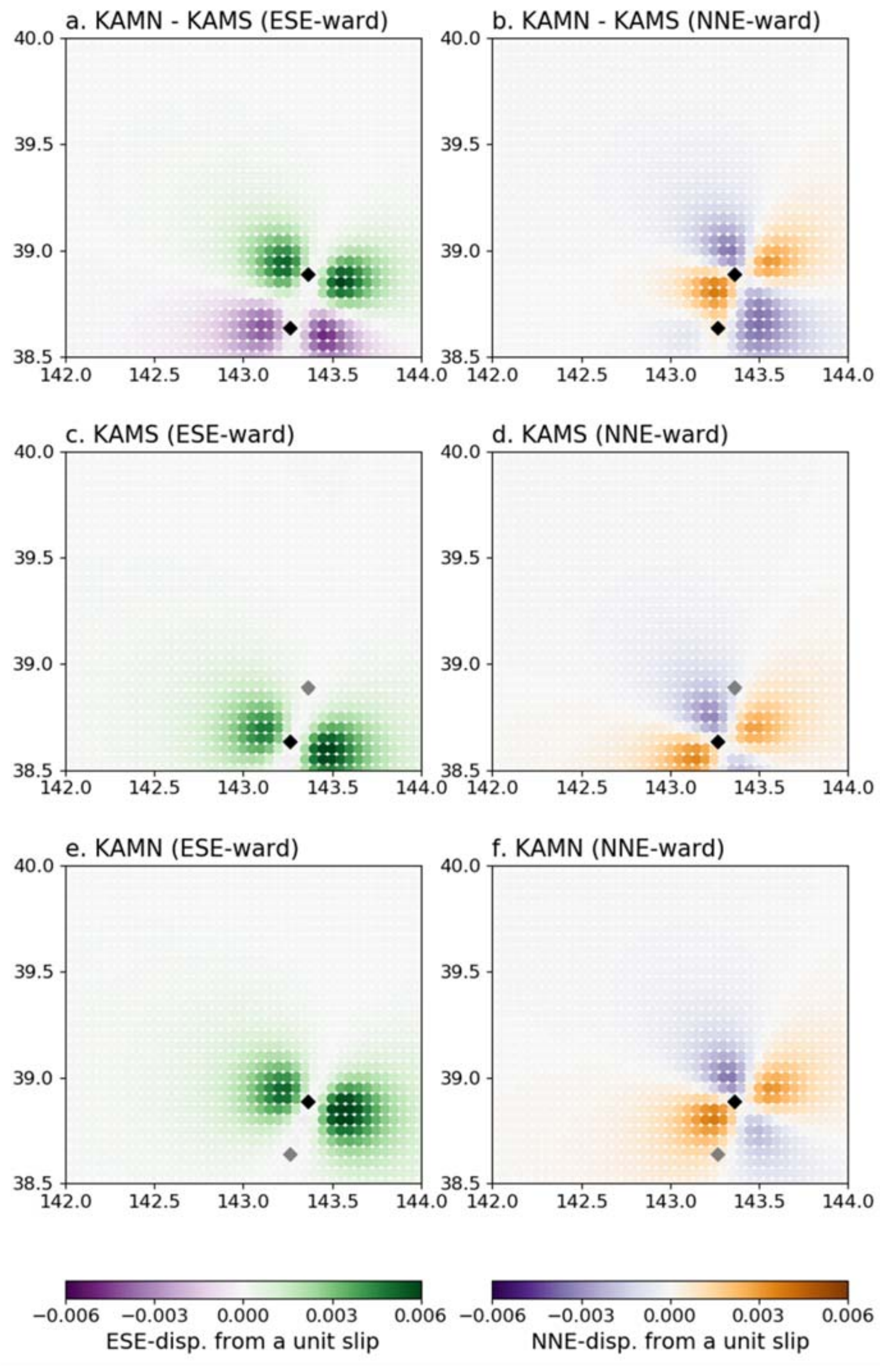


**Figure S4.** Contributions of the subfaults to (a)–(b) relative horizontal displacement at KAMN relative to KAMS, and (c)–(f) horizontal displacements at KAMN and KAMS. Strike, dip, and rake angles of the subfaults are fixed to 195°, 13°, and 90°, respectively. Black and gray squares indicate the locations of GNSS-A sites (KAMN and KAMS) in concern and not in concern in the panel, respectively.

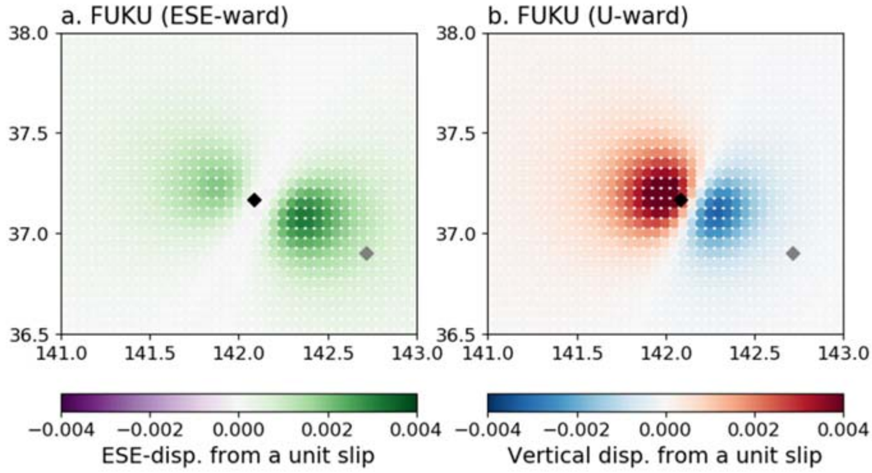


**Figure S5.** Contributions of the subfaults to (a) ESE-ward and (b) upward displacements at FUKU. Strike, dip, and rake angles of the subfaults are fixed to 200°, 13°, and 90°, respectively. Black and gray squares indicate the locations of FUKU and G17, respectively.

**Table S1.** Reference locations of GNSS-A sites.

| Site | Longitude (°E) | Latitude (°N) |
|---|---|---|
| KAMN | 143.363 | 38.886 |
| KAMS | 143.263 | 38.636 |
| MYGI | 142.917 | 38.083 |
| MYGW | 142.433 | 38.150 |
| FUKU | 142.083 | 37.167 |
| CHOS | 141.669 | 35.503 |
| G08 | 143.643 | 38.720 |
| G10 | 143.483 | 38.300 |
| G12 | 143.533 | 38.020 |
| G14 | 142.775 | 37.892 |
| G17 | 142.717 | 36.900 |

**References for this file**


Argus DF, Gordon RG, DeMets C (2011) Geologically current motion of 56 plates relative to the no-net-rotation reference frame. *Geochem Geophys Geosyst*, 12:Q11001. doi:10.1029/2011GC003751

Honsho C, Kido M, Tomita F, Uchida N (2019) Offshore postseismic deformation of the 2011 Tohoku earthquake revisited: Application of an improved GPS-acoustic positioning method considering horizontal gradient of sound speed structure. *J Geophys Res Solid Earth* 124:5990–6009. doi:10.1029/2018JB017135

Nakajima J, Hasegawa A (2006) Anomalous low-velocity zone and linear alignment of seismicity along it in the subducted Pacific slab beneath Kanto, Japan: Reactivation of subducted fracture zone?. *Geophys Res Lett* 33:L16309. doi:10.1029/2006GL026773

Nakamura Y, Yokota Y, Ishikawa T, Watanabe S (2021) Optimal transponder array and survey line configurations for GNSS-A observation evaluated by numerical simulation. *Front Earth Sci* 9:600993. doi:10.3389/feart.2021.600993

Okada Y (1992) Internal deformation due to shear and tensile faults in a half-space. *Bull Seism Soc Am* 82:1018-1040